

Coupled Quintessence scalar field model in light of observational datasets

Trupti Patil^a Ruchika^{b,c,1} Sukanta Panda^d

^{a,d}Department of Physics, Indian Institute of Science Education and Research Bhopal, Bhopal Bypass Road, Bhauri, Bhopal - 462066, Madhya Pradesh, India

^bDepartment of Physics, Indian Institute of Technology Bombay, Main Gate Road, Powai, Mumbai, Maharashtra 400076, India

^cPhysics Department and INFN, Università di Roma “La Sapienza”, Ple Aldo Moro 2, 00185, Rome, Italy

E-mail: trupti19@iiserb.ac.in, ruchika.ruchika@roma1.infn.it, sukanta@iiserb.ac.in

Abstract. We do a detailed analysis of a well-theoretically motivated interacting dark energy scalar field model with a time-varying interaction term. Using current cosmological datasets from CMB, BAO, Type Ia Supernova, $H(z)$ measurements from cosmic chronometers, angular diameter measurements from Megamasers, growth measurements, and local SH0ES measurements, we found that dark energy component may act differently than a cosmological constant at early times. The observational data also does not disfavor a small interaction between dark energy and dark matter at late times. When using all these datasets in combination, our value of H_0 agrees well with SH0ES results but in 2.5σ tension with Planck results. We also did AIC and BIC analysis, and we found that the cosmological data prefer coupled quintessence model over Λ CDM, although the chi-square per number of degrees of freedom test prefers the latter.

¹Corresponding author.

Contents

1	Introduction	1
2	Coupled field model and the Background dynamics	2
3	Linear Perturbation Equation	5
4	Observational data	5
5	Results and Discussion	6
5.1	<i>The H_0 and σ_8 Plane</i>	8
5.2	<i>The h-r_{drag} Plane</i>	10
5.3	<i>The S_8-Ω_{dm} Plane</i>	11
5.4	<i>The Co-moving Hubble Parameter</i>	12
5.5	<i>Other Cosmological Parameters</i>	12
5.6	<i>Comparison with ΛCDM results</i>	13
5.7	<i>Model Selection Statistics</i>	14
6	Final Remarks	14

1 Introduction

The significant observational evidence about Universe's dynamics [1–3] hint at the accelerated expansion at present. The elementary candidate to reveal the nature of this new physics includes Einstein's cosmological constant ' Λ ' with the equation of state (EoS) ' $\omega' = -1$ in the Λ CDM model. Though this model provides a good fit to the latest observations, it lacks solutions to other significant problems [4] in cosmology, especially to the fine-tuning problem and cosmic coincidence problem, also known as famous *Why now?* problem. Along with this, we still have no information about the nature of Dark Energy and Dark Matter. All we know is that our universe is composed of two types of perfect fluids, one of which is baryonic and responsible for the deceleration of the universe and the growth of structures. The other one, dominant at late times, has negative pressure and is responsible for the acceleration of the present universe. Both the components have different equation of state parameter $\omega = P/\rho$. The baryonic component is known to be like radiation-dominated, stiff matter, or the dust-like universe. However, the determination of the equation of state for dark energy (ω_{DE}) is still one of the important unresolved questions in cosmology. Recent studies [5–9] rules out the possibility of $\omega_{DE} \ll -1$ and other studies, SDSS and WMAP, [10] and [11] put bounds as $-1.67 < \omega_{DE} < -0.62$ and $-1.33 < \omega_{DE} < -0.79$ at present respectively.

Very recent results [12] and [13] very clearly rule out the possibility of rigid Λ by 5σ . In a complete cosmology model-independent way, the authors [14] showed at present, the universe requires a phantom equation of state ($\omega_{DE} < -1$) to explain the present observational datasets.

Thus, probing the cosmologists to explore beyond the standard model for dark energy candidates, perhaps dynamical dark energy model with varying EoS (ω), see [15–18], and references therein. The simplest possibility consists of a light scalar field such as a quintessence field, varying slowly during the Hubble time and can drive the accelerated expansion [19–24]. Some studies also argue that the quintessence scalar field should couple (non-gravitationally) with the matter as provided by [25] unless some special symmetry inhibits the coupling. Such a coupling or interaction between Dark Energy (DE)/quintessence scalar field and Dark Matter (DM) can be characterized by a continuous energy flow or momenta between the two components. Many studies in the literature prescribe a

purely phenomenological approach to deal with interacting cosmologies of dark sectors. Then, other classes of models are motivated from a field theory perspective and are well motivated. Numerous observations [26–37] are in support of the theory of dark sector interaction, constraining energy transfer from DM to DE or the opposite paved their way into existence. Cosmological observations indicate that the coupling impacts the universe’s evolution [38, 39]. Effects of interaction on the CMB and linear matter power spectrum [40, 41] (for detailed review [42]), the structure formation at different scales and times and halo mass function [43–47] and on the behavior of the cosmological parameters [48–51] have been investigated in respective works. Based on these, coupled quintessence models were also studied theoretically in several other contexts [52–57] to provide a viable cosmological solution. Interacting Dark Energy Models have also been studied extensively to alleviate "Hubble Tension" - which is now confirmed to be more than 5σ after SH0ES 2022 results [13, 58–60]. Along with Hubble Tension is coupled the S_8 tension or r_{drag} tension, i.e., the sound horizon at the drag epoch tension because BAO and CMB measure the product of H_0 and r_{drag} and not r_{drag} alone [61, 62]. Several works [34, 42, 63–77] tried to address these tensions in cosmology but could only solve one tension or the other by keeping the same number of parameters. The only solutions [65, 78–85] to resolve all cosmological tensions at present are those which are extremely fine-tuned or have more parameters and therefore increasing the uncertainties in the parameter space.

In the present work, we do a detailed and elaborate study of late-time cosmological dynamics. We mainly study the well-motivated dark matter and dark energy interaction case theoretically and try to understand how current observational data sets like CMB, Type Ia Supernovae, cosmic chronometers, BAO, Masers, growth rate data, and local H_0 measurement from SH0ES study influences the constraints on different cosmological parameters.

The work is structured as follows. In the next section, we present the model framework for the coupled dark sector and discuss its dynamics in brief. Later, we work out the linear dark matter perturbation evolution equation in section 3. Section 4 describes the observational data and methodology adopted in this work. Section 5 presents the results and thorough discussion from the observational analysis. We conclude the findings in Section 6.

2 Coupled field model and the Background dynamics

In our study, we assume that the geometry of the universe describing flat, isotropic, and homogeneous universe is given by Friedmann-Lemaître-Robertson-Walker (FLRW) metric and the line element for it is given by

$$ds^2 = -dt^2 + a^2(t)(dx^2 + dy^2 + dz^2). \quad (2.1)$$

which when transformed into spherical coordinates reads as

$$ds^2 = g_{\mu\nu}dx^\mu dx^\nu = -dt^2 + a^2(t)\left(\frac{dr^2}{1-kr^2} + r^2 d\theta^2 + r^2 \sin^2\theta d\phi^2\right). \quad (2.2)$$

where $k = -1, 0,$ and 1 denotes open, flat, and spatially closed universe. We consider a canonical scalar field ϕ (as dark energy component) and non-relativistic (cold) dark matter component with pressure $P_{dm} = 0$ undergoing an interaction that leads to a coupled quintessence dark energy model. Under this assumption, the action for dark sector coupling can be set up as

$$S = \int d^4x \sqrt{-g} \left(\frac{R}{2} - \frac{1}{2} g^{\mu\nu} \partial_\mu \phi \partial_\nu \phi - V(\phi) + \sum_i \mathcal{L}_m^i(\chi_i, \phi) \right). \quad (2.3)$$

\mathcal{L}_m is the matter Lagrangian for different matter field species, which also depends on the field ϕ through the coupling. Different matter species (i) may experience different couplings [86, 87]. However, radiation is assumed uncoupled to dark energy because of conformal invariance. We also ne-

glect the baryons since coupling to the baryons is strongly constrained by the local gravity measurements [88]. Thus, our study assumes that only dark matter couples to the dark energy scalar field. By taking varying the action (2.3) w.r.t. the inverse metric, we get Einstein's gravitational field equation as follows

$$G_{\mu\nu} = T_{\mu\nu} \equiv T_{\mu\nu}^{(\phi)} + T_{\mu\nu}^{(m)}. \quad (2.4)$$

where $T_{\mu\nu}$ is the sum of $T_{\mu\nu}^{(\phi)}$ (energy-momentum tensor of DE component) and $T_{\mu\nu}^{(m)}$ (energy-momentum tensor of matter component). Since we allow interaction between the dark species, they do not evolve independently but coupled. Furthermore, they satisfy the local conservation equation in the form given:

$$-\nabla^\mu T_{\mu\nu}^{(\phi)} = Q_\nu = \nabla^\mu T_{\mu\nu}^{(dm)}, \quad (2.5)$$

where Q_ν expresses the interaction between dark matter and dark energy.

$$Q_\nu = F_{,\phi} \rho_{dm} \nabla_\nu \phi, \quad (2.6)$$

in which $F_{,\phi} \equiv \partial F / \partial \phi$. $F(\phi) = F_0 \exp(\beta\phi)$ is the coupling strength. β is a constant. The radiation component, on the other hand, being not interactive with dark species, is separately conserved and follows $\nabla^\mu T_{\mu\nu}^{(r)} = 0$. Using the Einstein equations, Friedmann equations for the coupled case scenario can be expressed as

$$\begin{aligned} 3H^2 &= \frac{\dot{\phi}^2}{2} + V(\phi) + F(\phi)\rho_{dm} + \rho_r, \\ 3H^2 + 2\dot{H} &= -\left(\frac{\dot{\phi}^2}{2} - V(\phi) + F(\phi)P_{dm} + P_r\right). \end{aligned} \quad (2.7)$$

From the conservation of energy-momentum tensor (2.6) or equivalently from equation (2.7), one can easily derive energy conservation or continuity equation for each component.

$$\begin{aligned} \dot{\rho}_\phi + 3H\rho_\phi(1 + \omega_\phi) &= Q \\ \dot{\rho}'_{dm} + 3H\rho'_{dm} &= -Q \\ \dot{\rho}_r + 3H\rho_r(1 + \omega_r) &= 0 \end{aligned} \quad (2.8)$$

where $H \equiv \frac{\dot{a}}{a}$, indicates the time evolution of the universe. The dot indicates derivative with respect to time t , and $\rho'_{dm} = F(\phi)\rho_{dm}$ denotes the energy density of dark matter. Corresponding time component of interaction term in Eq.(2.6) is given by $Q = F_{,\phi}\rho_{dm}\dot{\phi}$.

To study the dynamics of cosmological scalar fields in the presence of background fluid, it is easier to work with dimensionless variables. In our case, we introduce

$$x = \frac{\phi'}{\sqrt{6}}, \quad y = \frac{\sqrt{V(\phi)}}{\sqrt{3}H}, \quad \Omega_{dm} = \frac{F(\phi)\rho_{dm}}{3H^2}, \quad \Omega_r = \frac{\rho_r}{3H^2}. \quad (2.9)$$

along with

$$\lambda = -\frac{V_{,\phi}}{V(\phi)}, \quad m = \frac{F_{,\phi}}{F(\phi)}.$$

where 'prime' denotes derivative w.r.t. $\ln(a)$. And we define energy fraction for dark energy as

$$\Omega_\phi = x^2 + y^2$$

and dark matter energy density as

$$\Omega_{dm} = 1 - (x^2 + y^2) - \Omega_r \quad (2.10)$$

satisfying $\Omega_\phi + \Omega_{dm} + \Omega_r = 1$. We introduce one another dimensionless quantity ‘ γ ’ for describing dark energy equation of state ‘ ω_ϕ ’ as:

$$\gamma = 1 + \omega_\phi = \frac{2x^2}{x^2 + y^2}. \quad (2.11)$$

Also, total (effective) equation of state parameter ‘ ω_{eff} ’ becomes

$$\omega_{eff} = x^2 - y^2 + \frac{\Omega_r}{3} \quad (2.12)$$

The coupled dynamical set of equations can now be expressed as:

$$\begin{aligned} \gamma' &= (2 - \gamma) \sqrt{3\gamma\Omega_\phi} \left(-\sqrt{3\gamma\Omega_\phi} + \lambda\Omega_\phi + m(1 - \Omega_\phi - \Omega_r) \right), \\ \Omega_\phi' &= 3(1 - \gamma)\Omega_\phi(1 - \Omega_\phi) + \Omega_\phi\Omega_r + m\sqrt{3\gamma\Omega_\phi}(1 - \Omega_\phi - \Omega_r), \\ \Omega_r' &= \Omega_r(\Omega_r - 1) + 3\Omega_r\Omega_\phi(\gamma - 1), \\ \lambda' &= -\sqrt{3\gamma\Omega_\phi}(\Gamma_\lambda - 1)\lambda^2, \\ m' &= \sqrt{3\gamma\Omega_\phi}(\Gamma_m - 1)m^2. \end{aligned} \quad (2.13)$$

where

$$\Gamma_\lambda = \frac{V_{,\phi\phi} V}{V_{,\phi}^2}, \quad \Gamma_m = \frac{F_{,\phi\phi} F}{F_{,\phi}^2}. \quad (2.14)$$

which for potential $V(\phi) \propto e^{-\lambda\phi}$ ($\lambda = \text{constant}$) and for coupling parameter $F(\phi) = F_0 \exp(\beta\phi)$ gives unity. To solve the above autonomous system set, we assume the initial value of ω_ϕ to be near -1, i.e., $\gamma \simeq 0.0001$ [24]. Other quantities, namely Ω_ϕ , Ω_r , λ , and m are free parameters.

Now, we study the dynamics of the system (2.13) with the stationary points which satisfy the constraint (2.10). The physically viable critical points (x_c , y_c , Ω_{dm_c}) are

$$P_1 = (0, 0, 0), \quad P_2^{(\pm)} = (\pm 1, 0, 0), \quad P_3^{(\pm)} = \left(\frac{\lambda}{\sqrt{6}}, \pm \sqrt{1 - \frac{\lambda^2}{6}}, 0 \right), \quad P_4^{(\pm)} = \left(\frac{2\sqrt{\frac{2}{3}}\lambda}{1 + \lambda^2}, \pm \frac{2\sqrt{1 + \frac{\lambda^2}{3}}}{1 + \lambda^2}, 0 \right).$$

Point P_1 explains the radiation-dominated universe as seen from Eq.(2.10) and takes the value of effective EoS parameter ω_{eff} as 1/3. Points $P_2^{(\pm)}$ describe the universe dominated by the kinetic part of the scalar field. Thus the solution corresponds to stiff fluid with the effective equation of state parameter $\omega_{eff} = \omega_\phi = 1$. Moreover, stationary points $P_3^{(\pm)}$ describe an accelerated universe when $|\lambda| < \sqrt{2}$. A corresponding de Sitter solution occurs only when $\lambda = 0$ making $\omega_{eff} = -1$, i.e., the field potential plays the part of the cosmological constant. Points $P_3^{(\pm)}$ are physically acceptable under the constraint $|\lambda| < \sqrt{6}$. However, points $P_4^{(\pm)}$ produces a dark energy dominated accelerated solution when $|\lambda| < (2\sqrt{2} - 1)$.

We now study the stability of the above stationary points. The following are the eigenvalues corresponding to the stationary points

$$e(P_1) = \left\{ 2, -1, \frac{1}{2} \right\}, \quad e(P_2^{(\pm)}) = \left\{ 3, \frac{1}{2}(3 \pm \sqrt{6}m), 3 \mp \sqrt{\frac{3}{2}}\lambda \right\},$$

$$e(P_3^{(\pm)}) = \left\{ \frac{\lambda^2}{2} - 3, \quad \lambda^2 - 3, \quad \frac{1}{2}(\lambda^2 + m\lambda - 3) \right\}, \quad e(P_4^{(\pm)}) = \left\{ \frac{1}{2} + \frac{2(m\lambda - 1)}{1 + \lambda^2}, \quad \frac{n \mp \sqrt{s}}{2(1 + \lambda^2)^2} \right\},$$

where, $n = 9 + \lambda^2 - 9\lambda^4 - \lambda^6$ and $s = 225 + 144\lambda^2 + 174\lambda^4 - 16\lambda^6 - 15\lambda^8$.

From the eigenvalues, we find that the point P_1 and the point $P_2^{(\pm)}$ exhibit saddle nature. Moreover, for $m = \lambda = 0$, point $P_2^{(\pm)}$ exhibits instability too. Point $P_3^{(\pm)}$ becomes a stable attractor for $\lambda^2 < 3$ and $m < \frac{3}{\lambda} - \lambda$ and it is a repeller when $\lambda^2 > 6$ and $m > \frac{3}{\lambda} - \lambda$. Otherwise, the point shows saddle behaviour. Furthermore, point $P_4^{(\pm)}$ acts as an attractor for $m < \frac{1}{4\lambda}(3 + \lambda^2)$ and $n < \sqrt{s}$ and becomes unstable when $m > \frac{1}{4\lambda}(3 + \lambda^2)$ and $n > -\sqrt{s}$. Point $P_4^{(\pm)}$ can also describe an oscillatory solution if 's' value becomes negative.

With these results, we now continue to investigate the perturbation theory for this model and its implications when confronted with cosmological observations.

3 Linear Perturbation Equation

Since the coupling modifies the evolution of matter perturbations and the clustering properties of galaxies, to gain further insight, we now study the evolution of the matter perturbations and, thence, include the linear growth rate data ($f\sigma_8$) from large-scale structure (LSS) survey. We re-scale the term " $F(\phi)\rho_{dm}$ " as ρ_c . Given this, we define the perturbation variable as $\delta_c \equiv \frac{\delta\rho_c}{\rho_c}$, where the subscript c stands for the (cold) dark matter component and $\delta\rho_c$ is the deviation from the background dark matter density. Mathematically, the equation governing the growth of perturbation (in the Newtonian gauge) at linear regime is given as

$$\delta_c'' + \left(2 + \frac{H'}{H}\right)\delta_c' - \frac{3}{2}\Omega_{dm}\delta_c = 0. \quad (3.1)$$

The introduction of coupling to the dark matter then modify the growth of matter perturbation as

$$\delta_c'' + \delta_c' \left(2 + \frac{H'}{H} - \frac{F_{,\phi}}{F(\phi)}\phi'\right) - \frac{3}{2}\delta_c \left(\Omega_{dm} - \frac{1}{3}\phi'^2\right) \left(1 + \frac{2F_{,\phi}^2}{F(\phi)^2}\right) = 0. \quad (3.2)$$

which can also be written in terms of dimensionless variables as

$$\delta_c'' = -\left(\frac{1}{2} - \frac{1}{2}\Omega_r - \frac{3}{2}(\gamma - 1)\Omega_\phi - m\sqrt{3\gamma\Omega_\phi}\right)\delta_c' + \frac{3}{2}\left(1 - \Omega_\phi(1 + \gamma) - \Omega_r\right)(1 + 2m^2)\delta_c. \quad (3.3)$$

We write the modified Hubble normalized, in terms of $N = \ln a$ as

$$\frac{H}{H_0} = \left[\Omega_{0,\phi}e^{-3N(1+\omega_\phi)} + \Omega_{0,dm}e^{-3N}e^{-m\sqrt{3\gamma\Omega_\phi}N} + \Omega_{0,r}e^{-4N}\right]^{\frac{1}{2}}. \quad (3.4)$$

The dark matter perturbations and the Hubble evolution for the uncoupled case are reproduced by setting $m = 0$. We consider the time evolution of the universe at $N_i = -7$ to ensure the evolution around the matter-dominated epoch. Therefore, we use the initial conditions as $\phi(N_i) = \phi'(N_i) = 0$. And for the matter density contrast we take $\delta_c(N_i) = \delta_c'(N_i) = 10^{-3}$. The dynamical set of equations (Eq. 2.13) and the perturbation equation (Eq. 3.3) are addressed with the cosmological observations to constrain the interacting scalar field quintessence model and its parameters.

4 Observational data

We devote this section to presenting and describing the main observational data implemented to constrain the model parameters and the statistical analysis results.

- The **Cosmic Microwave Background** (CMB) data are an effective probe for observational analysis of the cosmological models. In this work, we work with the CMB distance priors on the acoustic scale l_A leading to the alteration of the peak spacing and on the shift parameter ‘R’ affecting the heights of the peaks. We consider using the *Planck* 2018 compressed likelihood TT, TE, EE + lowE obtained by Chen et al [89] (see Ade et al. [90] for the detailed method for obtaining the compressed likelihood).
- For **SN** data, we use the SNe Ia samples of 1701 light curves of 1550 distinct Type Ia supernovae (SNe Ia) in the redshift range $z \in [0.001, 2.26]$ from the latest Pantheon+ compilation [91, 92]. This sample also includes SH0ES Cepheid host distance anchors (Riess et al, denoted as R21 [93]). Thus, for H_0 , when combining it with Pantheon+, we use the PantheonPlusSH0ES likelihood (refer Eq. 15 of [92]), where the Cepheid calibrated host-galaxy distance provided by SH0ES facilitates constraints on H_0 .
- The **cosmic chronometers** (CC) approach allows us to obtain observational values of the Hubble function at different redshifts $z \leq 2$ directly. Since these measurements are independent of any cosmological model and Cepheid distance scale, they can be used to place better constraints on it. In the present analysis, we measure $H(z)$ using the CC covariance matrix [94–96].
- For **Baryon Acoustic Oscillations** (BAO) data, we use data points from the following observations:
Isotropic BAO measurements by 6dF galaxy survey ($z = 0.106$) [97], by SDSS DR7-MGS survey ($z = 0.15$) [98] and measurements by SDSS DR14-eBOSS quasar samples ($z = 1.52$) [99]. Measurement of BAO using Ly α samples jointly with quasar samples from the SDSS DR12 study [100]. We also consider anisotropic BAO measurements by BOSS DR12 galaxy sample at redshifts 0.38, 0.51, and 0.61 [101].
- The **H₂O Megamaser** (hereafter, “MASERS”) technique under the Megamaser Cosmology Project (MCP) leads to the direct measurement of the H_0 by measuring angular-diameter distances to galaxies UGC 3789, NGC 5765b, and NGC 4258 in the Hubble flow redshifts $z = 0.0116, 0.0340,$ and 0.0277 respectively. [102–106]. The technique is based only on geometry, independent of standard candles and the extra-galactic distance ladder, and may provide an accurate determination of H_0 .
- In addition to geometric probes, we use the **growth rate** ($f\sigma_8(z)$) data provided by various galaxy surveys as collected in [107] to constrain cosmological parameters.

Now, to constrain the free and derived parameters of this coupled cosmological scenario, we use the Markov Chain Monte Carlo (MCMC) technique, emcee: the MCMC Hammer [108]. We work with the following parameter space $\mathcal{P} \equiv \{\Omega_{\phi_i} * 10^{-9}, r_{drag}, \lambda_i, m_i, \Omega_{r_i}, h, \sigma_8\}$ during the statistical analyses and the priors employed on these cosmological parameters are enlisted in Table 1. The physical limits are intact where $\Omega_{\phi} > 0$, $\Omega_{dm} > 0$ and $\Omega_r > 0$. During our further analysis, the Hubble constant is assumed to be $H_0 = 100h \text{ km s}^{-1} \text{ Mpc}^{-1}$; hence, we define the dimensionless parameter h . We have fixed the baryon density parameter, Ω_{b_0} to be 0.045 according to CMB constraints from *Planck* (2018) [58], which is also in agreement with Big Bang Nucleosynthesis (BBN) constraints and n_s to be 0.96. One should note that we have chosen positive priors on the interaction parameter. However, the results do not change if we choose negative or bigger priors alternatively.

5 Results and Discussion

We start by discussing the results obtained within the interacting canonical context. In table 2, we present the mean values and the 1σ ranges of different cosmological parameters with both coupled and uncoupled scenarios.

<i>Parameters</i>	<i>Flat prior interval</i>
$\Omega_{\phi_i} * 10^{-9}$	[0.05, 4.0]
r_{drag}	[130, 180] Mpc
λ_i	[10^{-4} , 3.0]
m_i	[10^{-6} , 10^{-2}]
Ω_{r_i}	[0.09, 0.17]
h	[0.5, 0.9]
σ_8	[0.6, 1.0]
M	[-21.0, -18.0]

Table 1: Flat priors on various parameters of the coupled model.

<i>Parameters</i>	$\Omega_{\phi_i} * 10^{-9}$	r_{drag} (Mpc)	λ_i	m_i	Ω_{r_i}	Ω_{dm}	h	σ_8
CMB+CC+BAO+MASERS								
<i>Coupled</i>	$1.125^{+0.275}_{-0.264}$	$147.73^{+5.83}_{-5.86}$	$0.99^{+0.46}_{-0.82}$	$0.0010^{+0.00038}_{-0.00096}$	$0.151^{+0.0102}_{-0.0105}$	$0.317^{+0.0121}_{-0.0126}$	0.671 ± 0.028	Unconstrained
<i>Un-coupled</i>	1.448 ± 0.053	$150.28^{+5.61}_{-5.79}$	$0.64^{+0.447}_{-0.436}$	-	$0.153^{+0.0096}_{-0.0099}$	$0.311^{+0.0084}_{-0.0085}$	0.665 ± 0.026	Unconstrained
CMB+PantheonPlus+CC+BAO+MASERS								
<i>Coupled</i>	$1.073^{+0.285}_{-0.280}$	$148.53^{+6.21}_{-6.27}$	$0.83^{+0.46}_{-0.32}$	$0.0011^{+0.00040}_{-0.00110}$	$0.151^{+0.0101}_{-0.0103}$	0.314 ± 0.0074	$0.671^{+0.028}_{-0.027}$	Unconstrained
<i>Un-coupled</i>	1.441 ± 0.054	$150.30^{+5.69}_{-5.75}$	$0.70^{+0.414}_{-0.384}$	-	$0.153^{+0.0095}_{-0.0098}$	0.313 ± 0.0072	$0.665^{+0.026}_{-0.025}$	Unconstrained
CMB+PantheonPlus+CC+BAO+MASERS+ $f\sigma_8(z)$								
<i>Coupled</i>	$1.041^{+0.295}_{-0.290}$	$148.31^{+6.01}_{-5.95}$	$0.80^{+0.49}_{-0.34}$	$0.0012^{+0.00047}_{-0.00110}$	$0.150^{+0.0101}_{-0.0101}$	$0.314^{+0.0074}_{-0.0075}$	0.672 ± 0.027	$0.740^{+0.022}_{-0.023}$
<i>Un-coupled</i>	1.441 ± 0.053	$150.30^{+5.64}_{-5.79}$	$0.71^{+0.411}_{-0.373}$	-	$0.153^{+0.0096}_{-0.0097}$	$0.313^{+0.0073}_{-0.0072}$	$0.665^{+0.026}_{-0.025}$	0.740 ± 0.022
CMB+PantheonPlus+CC+BAO+MASERS+ $f\sigma_8(z)+H_0$								
<i>Coupled</i>	$1.086^{+0.288}_{-0.284}$	$139.03^{+3.16}_{-3.15}$	0.79 ± 0.43	$0.0011^{+0.00046}_{-0.00110}$	$0.134^{+0.0057}_{-0.0056}$	$0.313^{+0.0085}_{-0.0086}$	0.717 ± 0.015	0.741 ± 0.022
<i>Un-coupled</i>	1.476 ± 0.052	$139.85^{+3.08}_{-3.09}$	$0.52^{+0.374}_{-0.380}$	-	$0.135^{+0.0057}_{-0.0057}$	$0.310^{+0.0075}_{-0.0076}$	0.716 ± 0.015	0.740 ± 0.022

Table 2: Mean values with 68% confidence level (CL) errors on cosmological and free parameters within the interacting and non-interacting paradigm from various data combinations.

To see the effect of the inclusion of each data set in the coupled scenario on the constraint of each parameter, we refer to Fig.1, where we show 1-dimensional marginalized posterior distributions and the corresponding 2D contour plots at 68% and 95% confidence level (CL) for all independent parameters. We gradually added PantheonPlus, $f\sigma_8$, and H_0 to the data set combination BAO + Masers + CMB + CC (further renamed as BASE combination) and can see more constrained parameters by adding more datasets. We also see a similar effect in the non-coupling case, as shown in Fig. 2. Since constraints on parameters show not much difference in the case of coupled or un-coupled scenarios, we, from now onward, focus on further studying the coupled case.

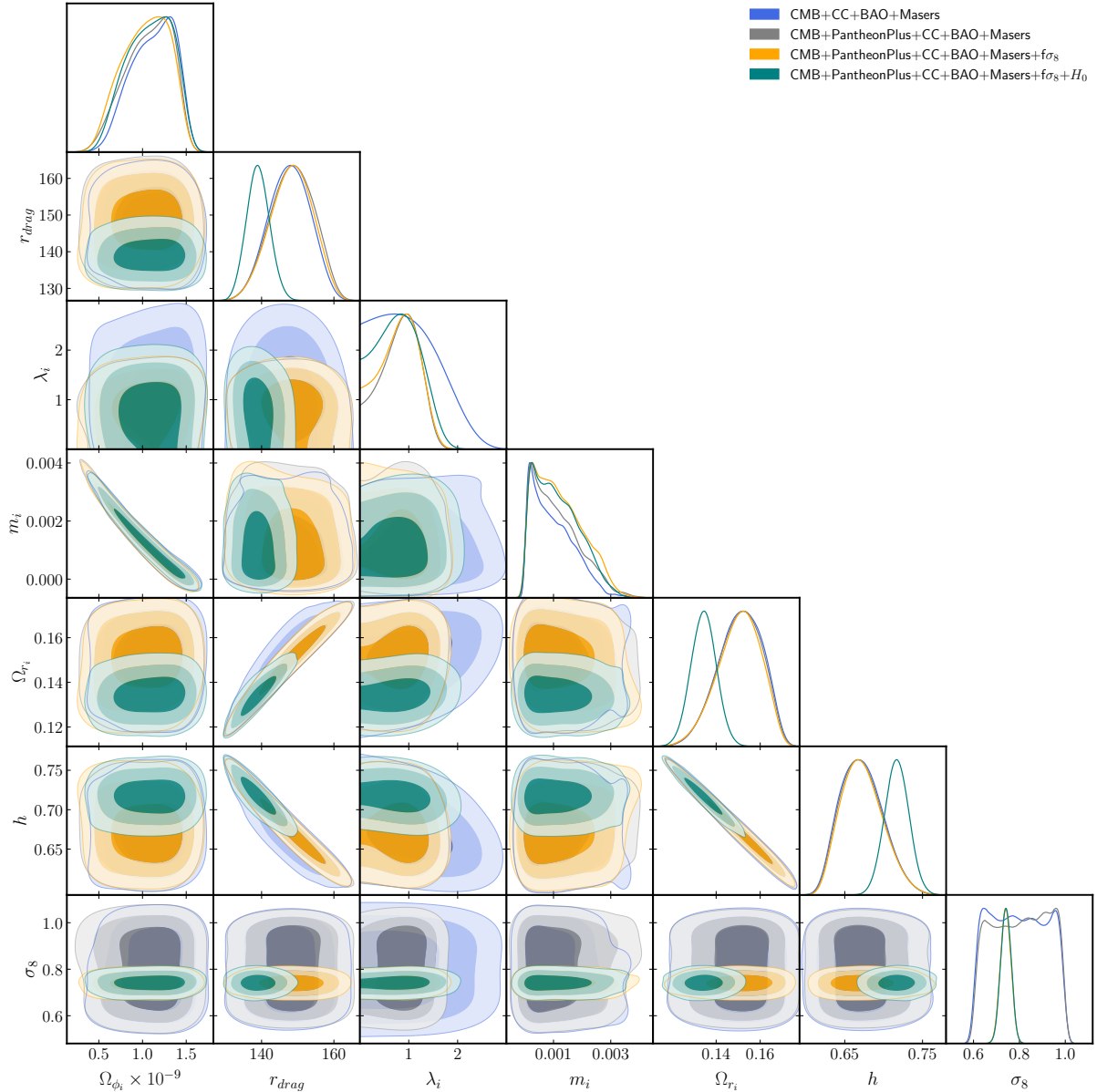


Figure 1: 68% and 95% CL contour plots and corresponding one-dimensional marginalized posterior distribution for all cosmological parameters obtained from the MCMC analysis within the present **coupling** scenario utilizing several combinations of data sets.

5.1 The H_0 and σ_8 Plane

We see that 1σ confidence level contours are relatively larger for CMB + CC + BAO + Masers (BASE) data than other data combinations. Whereas the addition of PantheonPlus sample significantly reduces the constraint on parameter Ω_{dm} , with the difference of $\sim 0.1\sigma$ to the BASE combination. This alteration estimates slightly higher uncertainty in r_{drag} , differing by less than 0.1σ relative to the BASE data. We also observe the change in the λ_i parameter with less than 0.3σ significance compared to the BASE combination, refer Table 2. Furthermore, the inclusion of $f\sigma_8$ and H_0 data to the previous data combination strongly reduces the parameter space on σ_8 and h , respectively, as seen in Fig. 1. Except parameter h and parameter σ_8 , we also find the notable impact on other parameters such as r_{drag} and λ_i when we add SH0ES data or when we include $f\sigma_8$ data in the analysis.

In this study, we found that CMB + CC + BAO + Masers (BASE) data combination shows $H_0 = 67.1 \pm 2.8$ km/s/Mpc at 68% CL which is compatible well within 0.3σ range with H_0 measurement

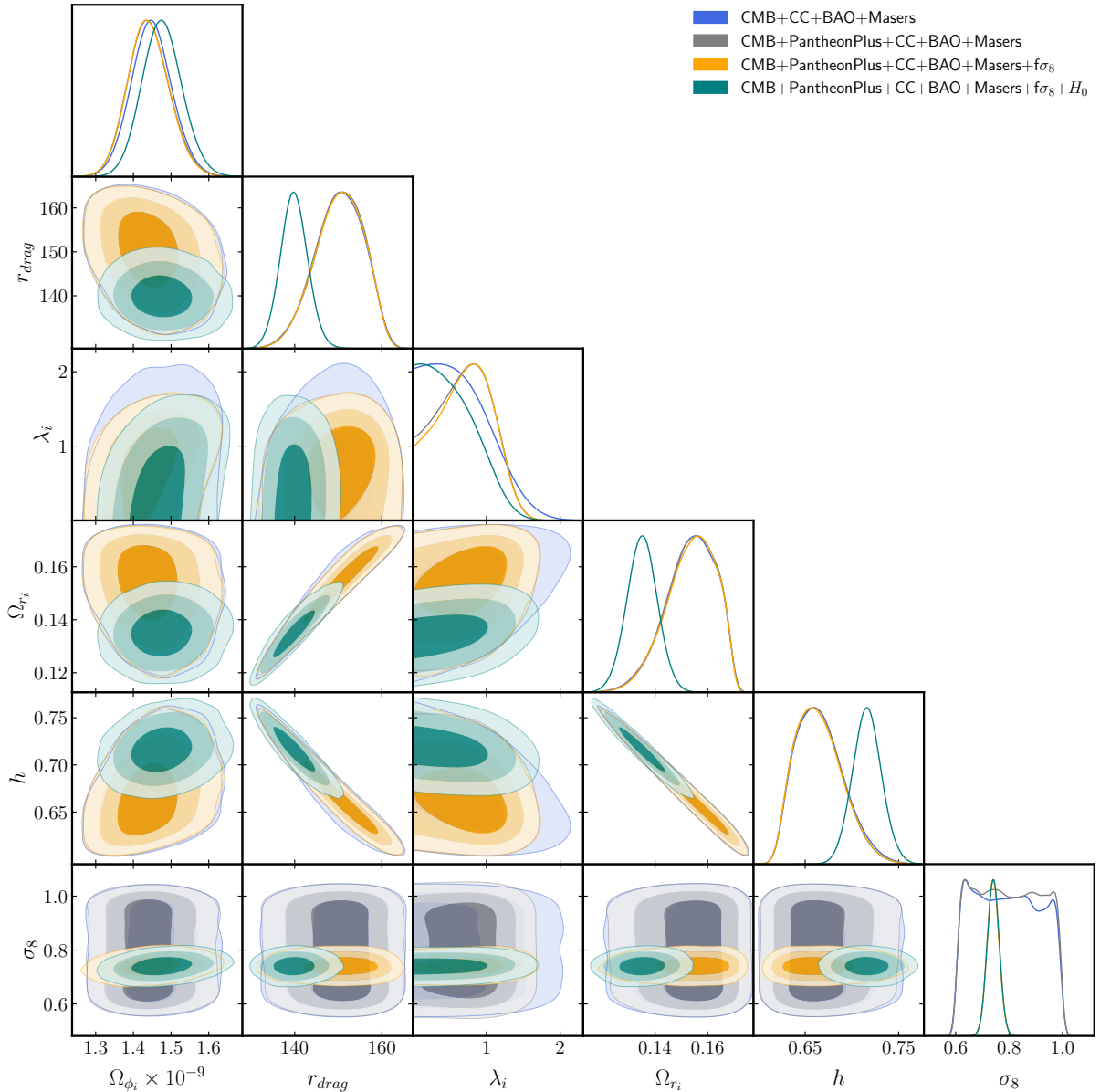


Figure 2: 68% and 95% CL contour plots and corresponding one-dimensional marginalized posterior distribution for all cosmological parameters obtained from the MCMC analysis for **non-coupling** scenario utilizing several combinations of data sets.

from the joint result using TT,TE,EE + lowE + lensing in *Planck* (2018) under Λ CDM ($H_0 = 67.37 \pm 0.54$ km/s/Mpc) [58]. But, the H_0 measurement from the same data combination shows 2σ discrepancy with the prediction from SH0ES measurement in R21 ($H_0 = 73.04 \pm 1.01$ km/s/Mpc) [93]. The consequent addition of PantheonPlus data and the analysis combining $f\sigma_8$ data produces essentially the same result for the Hubble constant as in the BASE combination. However, with the addition of H_0 data from SH0ES, we reached a determination of $H_0 = 71.7 \pm 1.54$ km/s/Mpc, 2.5σ increase in the difference from *Planck* (2018)+ Λ CDM of 67.37 ± 0.54 km/s/Mpc. The combined result of H_0 , 71.7 ± 1.54 km/s/Mpc, is consistent within $< 1\sigma$ (mildly greater than 0.5σ) range with the measurement of the Hubble constant, $H_0 = 73.04 \pm 1.01$ km/s/Mpc derived from the baseline fit with measurements from the latest SH0ES analysis in R21 [93].

We now present our multi-probe constraints on the structure growth parameter S_8 , using $S_8 = \sigma_8 \sqrt{\Omega_{dm_0}/0.3}$. As evident from Table 2, the σ_8 measurements from growth rate ($f\sigma_8$) data, along

	<i>Parameters</i>	Ω_{dm}	r_{drag} (Mpc)	h	$\Omega_{r_0} * 10^{-5}$	σ_8
<i>Data combinations</i>	CMB+CC+BAO+MASERS	$0.308^{+0.0078}_{-0.0076}$	$149.34^{+6.25}_{-6.24}$	0.674 ± 0.028	$5.41^{+0.398}_{-0.400}$	Unconstrained
	CMB+PantheonPlus+CC+BAO+MASERS	$0.312^{+0.0069}_{-0.0070}$	$149.16^{+6.36}_{-6.34}$	0.673 ± 0.028	$5.45^{+0.408}_{-0.403}$	Unconstrained
	CMB+PantheonPlus+CC+BAO+MASERS+ $f\sigma_8(z)$	$0.312^{+0.0070}_{-0.0071}$	$149.42^{+6.49}_{-6.48}$	$0.672^{+0.029}_{-0.028}$	$5.46^{+0.407}_{-0.415}$	0.736 ± 0.022
	CMB+PantheonPlus+CC+BAO+MASERS+ $f\sigma_8(z)+H_0$	0.309 ± 0.0073	$139.60^{+3.16}_{-3.12}$	0.719 ± 0.015	$4.79^{+0.219}_{-0.218}$	0.738 ± 0.022

Table 3: Mean values with 68% confidence level (CL) errors on cosmological and free parameters within the Λ CDM paradigm from various data combinations.

with CMB, SNIa, CC, BAO, MASERS, and H_0 data, are well constrained as compared to datasets that do not include $f\sigma_8$, i.e., “CMB + CC + BAO + MASERS” and “CMB + PantheonPlus + CC + BAO + MASERS” combinations. This discrepancy in σ_8 significantly impacts the reliability of the constraints on parameter S_8 for these data combinations (without $f\sigma_8$) because obtained S_8 solution arises from the parameter being unconstrained. Due to this, we refrain to present the constraints placed on S_8 for these combinations.

Advancing with $S_8 = \sigma_8 \sqrt{\Omega_{dm_0}/0.3}$, the addition of $f\sigma_8$ measurement yields systematically low value of S_8 and resulted in $S_8 = 0.758 \pm 0.023$ raising the difference with *Planck* (2018)+ Λ CDM ($S_8 = 0.830 \pm 0.013$) to precisely at 2σ . This prediction of S_8 is in excellent agreement with the KiDS-1000-BOSS results ($S_8 = 0.766^{+0.020}_{-0.014}$) [109], differing by 0.3σ . Whereas the estimation is in good agreement with DES-Y3 results ($S_8 = 0.776 \pm 0.017$) [110] with the difference of 0.5σ . The results from CMB + CC + BAO + Masers + PantheonPlus + $f\sigma_8(z)$ are more robust in tightening constraints on the σ_8 or the S_8 parameter and justify the reduced uncertainty and the parameter space compared to the results from without growth rate data combination; see Table 2 and Fig. 1. Finally, the combined data constraint yields $S_8 = 0.757 \pm 0.023$, a difference of 2.5σ from the results of *Planck* (2018)+ Λ CDM [58]. However, this analysis of combined data produces essentially the same results as in the previous analysis maintaining a good agreement of 0.3σ and 0.5σ with the measurements obtained from KiDS-1000-BOSS survey [109] and DES-Y3 survey [110], respectively.

To assess the robustness of our findings and to check for the ambiguity concerning the prior dependency in the obtained results we present the results with different priors on the cosmological parameters in Table 5 and in Table 7, in the Appendix. We found that the values of the key cosmological parameters (both mean and error bars) are independent of priors only when the $f\sigma_8$ is in consideration along with other data sets of CMB, SNIa, CC, BAO, MASERS, and H_0 . This is explained in detail in the Appendix.

5.2 The h - r_{drag} Plane

In addition to a discrepancy in the Hubble constant, there is a discrepancy in the co-moving sound horizon at the end of the baryon drag epoch, r_{drag} as well. The two parameters H_0 and r_{drag} are strictly related when we consider BAO observations. In actuality, a combination of expansion history probes such as BAO and PantheonPlus data can provide a model-independent estimate of the low-redshift standard ruler, constraining the product of h (with $H_0 = h \times 100$ km/s/Mpc) and the sound horizon r_{drag} directly. This implies that, to have a higher H_0 value in agreement with SH0ES, we need $r_{drag} \sim 137$ Mpc, while to agree with *Planck*, assuming Λ CDM, we need $r_{drag} \sim 147$ Mpc. For this reason, the solutions that increase the expansion rate and at the same time decrease r_{drag} are most promising. In our analysis, this feature is completely in agreement with the *Planck* (2018) estimates

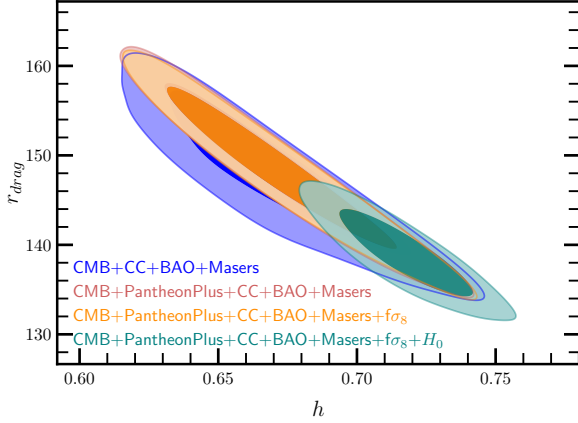


Figure 3: Constraints in the h - r_{drag} plane from different combination of CMB, CC, BAO, Masers, Pantheon, growth and H_0 data (68% and 95% contours) in case of interacting model.

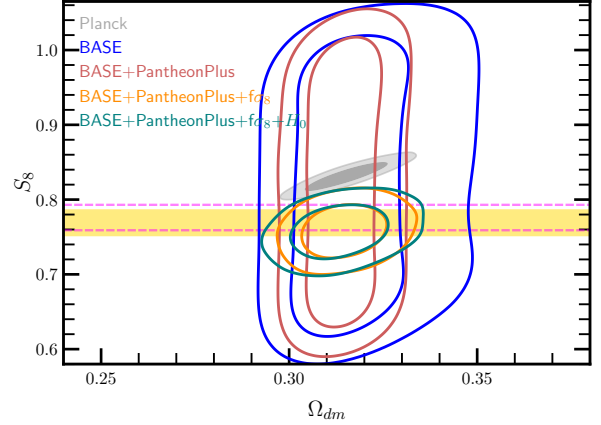


Figure 4: Marginalised constraints for the joint distributions of the fluctuation amplitude parameter S_8 and dark matter density parameter Ω_{dm} . The 68% and 95% credible regions are shown for different sets of CMB, SNIa, CC, BAO, MASERS, H_0 , and growth data for an interacting model. The golden band reflects the 68% credible interval for S_8 from the KiDS-1000-BOSS joint analysis whereas the region between pink dashed lines represent DES-Y3 results. For comparison, we also incorporated the *Planck* (2018) results (in grey contour). The BASE results are for “CMB + CC + BAO + Masers” dataset.

due to the strong compatibility of estimated H_0 with the one from *Planck* (2018) + Λ CDM model. However, the addition of SH0ES result gives $H_0 = 71.7 \pm 1.54$ km/s/Mpc, that is closer to the R21 value of H_0 , also leads to an empirical determination of r_{drag} near 139 Mpc. This modest discrepancy in the sound horizon value r_{drag} from the one in [111] agrees with the slight discrepancy in the H_0 measurements from SH0ES. This correlation can also be seen from table 2. Evidently, this cosmological solution is promising and consistent with the fact that the relation $h - r_{drag}$ is constant by the BAO measurements.

5.3 The S_8 - Ω_{dm} Plane

The model that allows larger H_0 values tend to introduce other tensions, such as higher S_8 values. To obtain simultaneously higher values of H_0 , lower values of S_8 , and consistent values of Ω_{dm} is also necessary to define the correct evolution. Since adding the BAO and SNe measurements to the *Planck* data strengthens the constraints towards *Planck* values, the correlation between their combined results is relatively strong. Referring to the Table 2, $f\sigma_8$ addition improves the S_8 consistency with KiDS-1000-BOSS [109] and DES-Y3 [110] results. This is also illustrated in Fig. 4. We, particularly, show that only dataset that includes $f\sigma_8$, constrain S_8 or σ_8 better while other datasets (without $f\sigma_8$) fails to put constrain on it. From this joint analysis, we found a lower and a well-constrained estimation for S_8 , leading to a lower and a constrained value for Ω_{dm} (Table 2 and Fig. 4). Moreover, using the full combined likelihood for the data considered in this work we found the similar results with further increment in the H_0 estimated value while S_8 retaining the consistency with KiDS-1000-BOSS and DES-Y3 survey results.

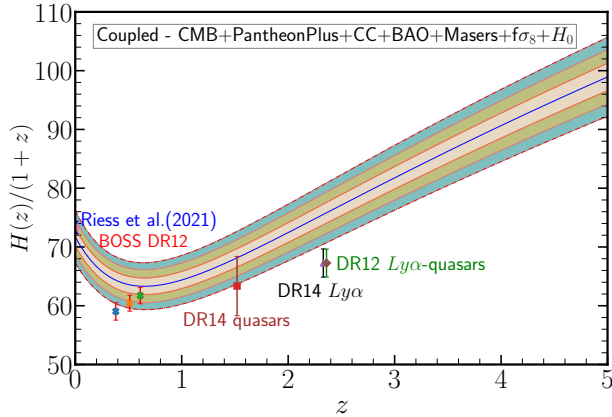


Figure 5: Co-moving Hubble parameter as a function of redshift, clearly showing the onset of acceleration just before the redshift around $z = 0.6$, reconstructed using a combination of CMB, SNIa, CC, BAO, Masers, H_0 and growth data for interacting model. The solid blue line shows the best-fit reconstructed results, while the outer regions show results within 1σ , 2σ , 3σ CL separated by orange, pink and red-dashed lines.

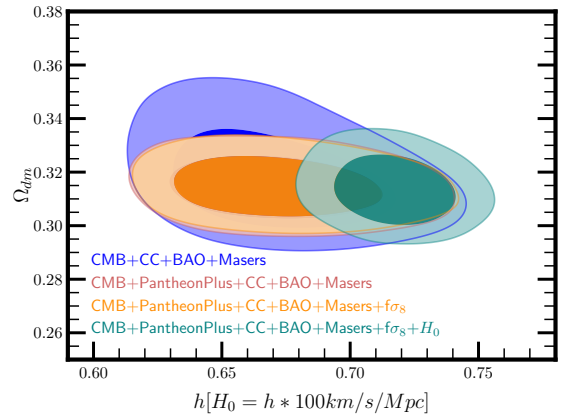


Figure 6: The CMB + SNIa + CC + BAO + Masers + $f\sigma_8 + H_0$ data constraints on h and Ω_{dm} in the coupled model, compared to the results from without H_0 data. Adding SH0ES H_0 constrains the Hubble parameter, comparable to that R21 estimation. Darker and lighter contours show 68% and 95% of the probability, respectively.

5.4 The Co-moving Hubble Parameter

The recent BAO measurements along the line of sight and transverse directions lead to joint constraints on $H(z)r_{drag}$. Since *Planck* + Λ CDM constrains r_{drag} to a precision of 0.2 %, the BAO measurements can be accurately converted into absolute measurements of $H(z)$. These constraints on $H(z)$ from the BOSS analyses are plotted in Fig. 5. The error bars are constraints from BOSS DR12 galaxy sample [101], eBOSS DR14 quasar sample [99], the correlations of $Ly\alpha$ absorption in eBOSS DR14 at $z = 2.34$ [112] and from the $Ly\alpha$ auto-correlation and cross-correlation with quasars from SDSS data release DR12 [100]. The error bar at $z = 0$ shows the inferred distance-ladder Hubble measurement from R21 [93].

The illustration in Fig. 5 shows clearly how well the dark energy interaction model fits the BAO measurements of the Hubble parameter except for the DR12 $Ly\alpha$ data point. It is also consistent with the R21 measurements of Hubble at $z = 0$ for all the data sets combined in this work within 1σ error bars. This is also illustrated in Fig. 6, which shows the combined constraints on h and Ω_{dm} from different data combinations. Without adding H_0 to the combination of CMB, BAO, Pantheon-Plus, $H(z)$, Masers, and $f\sigma_8$, the tension with SH0ES measurement of H_0 still prevails as seen in table 2, though the same results show lower mean value and well improved constraints on Ω_{dm} as compared to the BASE data. However, the addition of SH0ES data (green contour) constrain Ω_{dm} towards slightly lower mean value and shifts H_0 closer to the R21 measurement.

5.5 Other Cosmological Parameters

We further analyse the model for completeness' sake and clarity. We have plotted the energy density evolution parameter for dark energy and dark matter, along with 68% and 95% CL for the coupled case using all the data presented in this work in Fig. 7. Fig. 8 shows the overlapping confidence contours for the equation of state parameter as a function of redshift from coupled and uncoupled models using all the data presented in this work. The solid yellow and red lines indicate the best-fit values for the DE EoS parameter for coupled and uncoupled models, respectively. However, Fig. 9 shows the

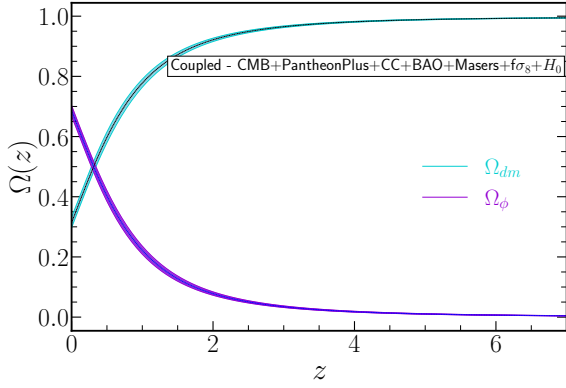


Figure 7: The 68% and 95% CL along with the mean value for relative energy density parameters Ω_{dm} (cyan) and Ω_{ϕ} (purple) for the coupled model with respect to redshift (z). The evolution is plotted for all the data combined together, considered in this work. The black-dashed and blue-dashed lines corresponds to the best-fit values of DM and DE density parameters.

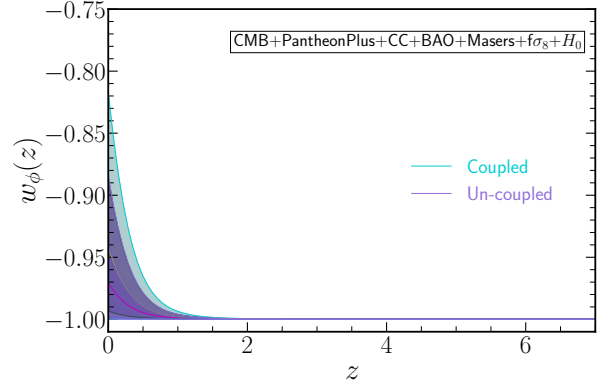


Figure 8: Evolution of dark energy equation of state parameter with respect to redshift (z) for coupled and un-coupled scenario. The solid yellow line shows the best fit result while the outer blue and cyan regions show the 1σ and 2σ CL for coupled case. The solid red line shows the best fit result while the outer purple regions show the 1σ and 2σ CL for un-coupled case.

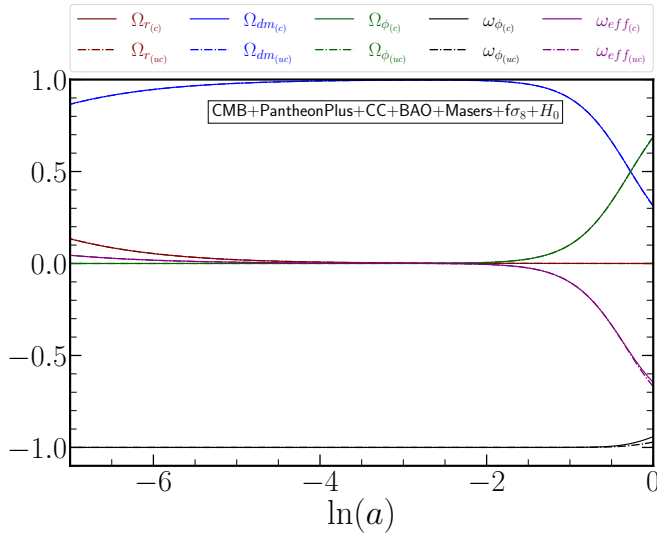


Figure 9: The best-fit evolution of key cosmological parameters for the coupled and uncoupled models is shown for the combined set of CMB, SNIa, CC, BAO, Masers, H_0 , and growth data. The solid lines and dashed-dotted lines show the evolution in the coupled case and un-coupled case, respectively.

density parameters and equation of state parameters evolution from their best-fit values as a function of the logarithmic scale factor. These analyses exactly show the expected behaviour of the observed universe at present, which is dark energy-dominated accelerated expansion. Moreover, while fitting with the data, we found that the model favors small values of the coupling parameter “ Q ”, making the parameter evolution indistinguishable compared to the one from the uncoupled case. However, these predictions are model-dependent and may vary for other coupling models.

5.6 Comparison with Λ CDM results

In Table 3, we present the constraints that we got from χ^2 minimization fitting assuming the standard Λ CDM model. We also show how the mean values change within the same model in addition to different datasets. We observe the notable impact on the addition of PantheonPlus sample to the BASE combination that significantly changes the parameter, Ω_{dm} values (both mean and error bars). These changes narrow down the Ω_{dm} parameter space. Growth rate ($f\sigma_8(z)$) data addition reflects

more precised constraint on σ_8 or S_8 parameter compared to “CMB + PantheonPlus + CC + BAO + Masers” data set, keeping other parameters unaltered. Further inclusion of local H_0 value from SH0ES shifts the mean value of h towards Riess et al. value [13] with smaller error bars, differing by $\sim 1.5\sigma$ relative to the h value obtained from without SH0ES data sets. The effect of the shift in h can also be seen in r_{drag} parameter values (both mean and reduced error bars) and in Ω_{dm} parameter value with lower mean.

5.7 Model Selection Statistics

In this section, we discuss the comparison of our models (coupled and uncoupled) with the standard Λ CDM model. The Λ CDM model corresponds to the dark energy equation of state -1, whereas in our model, the dark energy equation of state is allowed to vary. One way to compare these dark energy models is Akaike Information Criterion (AIC), where AIC is defined as $AIC = \chi_{min}^2 + 2 \cdot d$. Another way is Bayesian Information Criterion (BIC), where BIC is defined as $BIC = \chi_{min}^2 + d \cdot \ln(N)$. χ_{min}^2 is the chi-squared minimization to measure how well the data fit a model. ‘d’ is the number of parameters in the model and ‘N’ is the number of observational data points. The lowest chi-squared and lowest AIC or BIC at each point indicate where the parameters and model most closely match the measured data. Comparing both the methods, we can see from table 4 that there is always an improvement in χ_{min}^2 value for the coupled model when compared to the un-coupled or Λ CDM model. For all the data together, this leads to a large reduction in AIC and BIC estimates for the coupled model, and hence, the same is significantly preferred over the Λ CDM model.

We also considered χ_{min}^2 per number of degrees of freedom approach for the present model, aiming to understand the observational solidity of the model with respect to the standard reference model. We found that $\frac{\chi_{min}^2}{n_{dof}}$ raises an over-fitting issue with the coupled model opposing the analysis from AIC. This trait can be found in Table 4. However, using $\frac{\chi_{min}^2}{n_{dof}}$ method, it is clear that the Λ CDM model has the goodness of fit (GoF) to the data and hence, is the favoured model. In summary, from the point of view of the $\frac{\chi_{min}^2}{n_{dof}}$ analysis, Λ CDM is still a preferred candidate but from the perspective of AIC and BIC analyses, coupled cosmology is the preferred scenario for the universe’s evolution.

Model	χ_{min}^2	$\frac{\chi_{min}^2}{n_{dof}}$	d	N	AIC	BIC	Δ AIC	Δ BIC
Coupled	1216.063	0.699	8	1748	1232.063	1275.792	373.365	362.433
Un-coupled	1345.614	0.773	7	1748	1359.614	1397.877	245.814	240.348
ΛCDM	1593.428	0.912	6	1748	1605.428	1638.225	0.0	0.0

Table 4: The χ_{min}^2 , AIC and BIC estimation for coupled/un-coupled and Λ CDM model for the combination of all data set.

6 Final Remarks

In this work, we study an interacting dark energy-dark matter model having time-varying interaction term $Q = F_{,\phi} \rho_{dm} \dot{\phi}$. This work is interesting because it is theoretically very well motivated from a field theory perspective, not just phenomenological. We can see that because of the time-varying interaction term, the dark energy component may differ from the cosmological constant at very early times ($z = 1100$). Also, a small interaction is not disfavoured by the data at late times. However, we observed that there is no significant difference in the constraining power of the coupled model over the uncoupled one. We found that the parameter m_i which is the coupling parameter peaks at the

very lower value in the prior range provided, which makes the coupling significantly low making it indistinguishable from the uncoupled case.

Initially, we tested our model to find the future attractor solution by formulating a coupled dynamical set of equations. Later, we subjected the model to various data combinations and tried to understand better the influence of each cosmological data set on respective cosmological parameters.

We found that while using all the datasets together, we found H_0 value to be in excellent agreement with the latest local determination of H_0 by R21 [93], though in substantial ($\sim 2.5\sigma$) tension with *Planck* [58] measurements. It is widely discussed that the models that alleviate the H_0 discrepancy do not necessarily solve other tensions, such as a higher value of σ_8 or S_8 . Similarly, in our work, we found that the coupled model provides a remarkably better fit to the CMB, CC, BAO, Masers, PantheonPlus, $f\sigma_8$ and H_0 in combination with each other and predicts a (lower) late-time structure growth parameter $S_8 = 0.757 \pm 0.023$. The S_8 value is in good agreement with KiDS-1000-BOSS and DES-Y3 estimations, although in moderate tension with *Planck* 2018 + Λ CDM results which prefer a roughly 2.5σ higher value of S_8 compared to our model prediction.

We also emphasize the parameters like the sound horizon at the drag epoch r_{drag} and the dark matter energy density Ω_{dm} , and their respective correlations, in terms of $h-r_{drag}$ and $S_8-\Omega_{dm}$ planes. The findings predicted the smaller value of r_{drag} for a larger value of H_0 at the cost of increasing disagreement with the *Planck* data estimates. Moreover, the results from the $S_8-\Omega_{dm}$ parameter space showed marginal tension with *Planck* with lower and constrained values of S_8 and Ω_{dm} for all the combined data in this work. The illustration in Fig. 5 clearly showed some disagreement ($\sim 3\sigma$) with high-redshift BAO measurements from quasar Ly α observations. The interacting model confirms the overall good consistency of reconstructed $H(z)$ with combined BAO measurements of $H(z)$. Later, we also presented the time evolution of key cosmological parameters along with their confidence ranges for the coupled cosmological model. We found no significant distinction in the parameter evolution compared with the uncoupled scenario due to very low coupling parameter values preferred by the cosmological datasets. Later, we also presented the time evolution of density parameters, the equation of state parameters, and their two-sigma confidence region for the coupled cosmological model.

We then discussed the model comparison techniques to measure the goodness of fit of a given model to the data. We found that introducing extra parameters improves the fit determined by AIC and BIC and strongly favors a complex, coupled model over the Λ CDM one. Moreover, this model introduces two extra parameters, so the “weighted” chi-square test favors the Λ CDM for all the combined data. Such inconsistencies and discrepancies motivate us to look further for the best theoretical model to describe the universe. Following the above analyses, these differences could signify either the need for new exotic dark energy physics to withstand the data or new observations to improve the quality of the data.

In the near future, we shall extend our analysis to incorporate one extra element which can mimic phantom dark energy at present, along with the already present interacting dark matter-dark energy scenarios to resolve present cosmological tensions.

Acknowledgments

We thank the anonymous referee for their thoughtful remarks and suggestions which led to material improvements in the paper. We are grateful to Abhijith A., Shah Navaz Adil, Anjan Ananda Sen, Elsa M. Teixeira for useful discussions. Part of the numerical computation of this work was carried out on the computing cluster Pegasus of IUCAA, Pune, India. This work is partially supported by DST (Govt. of India) Grant No. SERB/PHY/2021057. Ruchika acknowledges TASP, iniziativa specifica INFN, for financial support.

Appendix

Here our aim is to show that our results are independent of priors only when $f\sigma_8$ data is considered. To validate this, we have obtained the results by changing the “ σ_8 ” range from $[0.6\sim 1]$ to $[0.5\sim 1]$, along with the updated priors (as shown in the Table 1). The obtained results are presented in Table 5. Here, we have noticed the similar behaviour in the results as in the case of Table 2, which shows the unconstrained σ_8 for its increased prior range, for combinations “CMB + CC + BAO + MASERS” and “CMB + PantheonPlus + CC + BAO + MASERS”. Thus, indicates the prior dependence of σ_8 when $f\sigma_8$ data is excluded.

However, for other combinations that include growth rate data ($f\sigma_8(z)$), the parameter, σ_8 as well as the other key parameters are well constrained and their values are independent of the priors, as can be seen from Table 2 and Table 5. Therefore, it can be concluded that the values of the key cosmological parameters are independent of priors only when the $f\sigma_8$ is in consideration along with other data sets of CMB, SNIa, CC, BAO, MASERS, and H_0 .

<i>Parameters</i>	$\Omega_{\phi_i} * 10^{-9}$	$r_{drag}(\text{Mpc})$	λ_i	m_i	Ω_{r_i}	Ω_{dm}	h	σ_8
CMB+CC+BAO+MASERS								
<i>Coupled</i>	$1.125^{+0.275}_{-0.264}$	$147.73^{+5.83}_{-5.86}$	$1.03^{+0.51}_{-0.77}$	$0.00099^{+0.00040}_{-0.00094}$	$0.151^{+0.0102}_{-0.0105}$	$0.318^{+0.0127}_{-0.0129}$	0.671 ± 0.028	Unconstrained
CMB+PantheonPlus+CC+BAO+MASERS								
<i>Coupled</i>	$1.085^{+0.283}_{-0.275}$	$148.35^{+6.06}_{-6.02}$	$0.81^{+0.49}_{-0.34}$	$0.00107^{+0.00040}_{-0.00100}$	$0.150^{+0.0100}_{-0.0099}$	0.314 ± 0.0076	0.672 ± 0.027	Unconstrained
CMB+PantheonPlus+CC+BAO+MASERS+ $f\sigma_8(z)$								
<i>Coupled</i>	$1.048^{+0.284}_{-0.282}$	$148.50^{+5.77}_{-5.87}$	$0.80^{+0.49}_{-0.36}$	$0.0012^{+0.00047}_{-0.00110}$	$0.151^{+0.0095}_{-0.0096}$	$0.314^{+0.0076}_{-0.0077}$	0.671 ± 0.026	$0.740^{+0.023}_{-0.022}$
CMB+PantheonPlus+CC+BAO+MASERS+ $f\sigma_8(z)+H_0$								
<i>Coupled</i>	$1.048^{+0.318}_{-0.307}$	$139.11^{+3.19}_{-3.15}$	0.79 ± 0.43	$0.0012^{+0.00051}_{-0.00120}$	$0.134^{+0.0058}_{-0.0057}$	$0.313^{+0.0084}_{-0.0085}$	$0.717^{+0.015}_{-0.016}$	0.741 ± 0.022

Table 5: Mean values with 68% confidence level (CL) errors on cosmological and free parameters within the interacting paradigm from various data combinations with updated σ_8 $[0.5\sim 1]$ prior.

To solidify above inference, we also show the results with different priors (considered in Table 6), on other cosmological parameters in Table 7, for comparison. By comparing with Table 2, we found that both the cases do not show any significant changes in key cosmological parameters such as h , r_{drag} , Ω_{dm} , and σ_8 values (both mean and error bars) for “CMB + PantheonPlus + CC + BAO + MASERS + $f\sigma_8(z)$ ” and “CMB + PantheonPlus + CC + BAO + MASERS + $f\sigma_8(z) + H_0$ ” combinations. Therefore, we can say that the σ_8 and other key cosmological parameters are well constrained and shows prior independence, given the growth rate data is present in the considered datasets.

<i>Parameters</i>	<i>Flat prior interval</i>
$\Omega_{\phi_i} * 10^{-9}$	[1, 3]
r_{drag}	[130, 180] Mpc
λ_i	$[10^{-3}, 1.5]$
m_i	$[10^{-5}, 10^{-3}]$
Ω_{r_i}	[0.09, 0.17]
h	[0.5, 0.9]
σ_8	[0.6, 1.0]

Table 6: Different priors on the parameters of the coupled model.

<i>Parameters</i>	$\Omega_{\phi_i} * 10^{-9}$	r_{drag} (Mpc)	λ_i	m_i	Ω_{r_i}	Ω_{dm}	h	σ_8
CMB+CC+BAO+MASERS								
Coupled	$1.128^{+0.153}_{-0.149}$	$148.21^{+6.00}_{-6.18}$	$0.74^{+0.42}_{-0.42}$	$0.00062^{+0.00028}_{-0.00053}$	$0.150^{+0.0099}_{-0.0104}$	$0.313^{+0.0089}_{-0.0091}$	0.674 ± 0.027	Unconstrained
CMB+PantheonPlus+CC+BAO+MASERS								
Coupled	$1.227^{+0.156}_{-0.151}$	$148.45^{+5.95}_{-6.04}$	$0.79^{+0.50}_{-0.29}$	$0.00062^{+0.00027}_{-0.00055}$	$0.151^{+0.0098}_{-0.0099}$	0.313 ± 0.0073	0.672 ± 0.027	Unconstrained
CMB+PantheonPlus+CC+BAO+MASERS+ $f\sigma_8(z)$								
Coupled	$1.228^{+0.156}_{-0.150}$	$148.37^{+5.96}_{-6.14}$	$0.79^{+0.49}_{-0.30}$	$0.00061^{+0.00026}_{-0.00055}$	$0.151^{+0.0100}_{-0.0102}$	0.314 ± 0.0071	0.672 ± 0.027	0.740 ± 0.022
CMB+PantheonPlus+CC+BAO+MASERS+ $f\sigma_8(z)+H_0$								
Coupled	$1.243^{+0.169}_{-0.165}$	$139.10^{+3.10}_{-3.08}$	$0.77^{+0.54}_{-0.33}$	$0.00066^{+0.00032}_{-0.00059}$	$0.134^{+0.0057}_{-0.0056}$	$0.312^{+0.0079}_{-0.0078}$	0.717 ± 0.015	0.742 ± 0.022

Table 7: Mean values with 68% confidence level (CL) errors on cosmological and free parameters within the interacting paradigm from various data combinations using priors listed in Table 6.

References

- [1] S. Perlmutter *et al.*, “Discovery of a supernova explosion at half the age of the Universe and its cosmological implications,” *Nature*, vol. 391, pp. 51–54, 1998.
- [2] A. G. Riess *et al.*, “Observational evidence from supernovae for an accelerating universe and a cosmological constant,” *Astron. J.*, vol. 116, pp. 1009–1038, 1998.
- [3] S. Perlmutter *et al.*, “Measurements of Ω and Λ from 42 high redshift supernovae,” *Astrophys. J.*, vol. 517, pp. 565–586, 1999.
- [4] P. J. E. Peebles and B. Ratra, “The Cosmological Constant and Dark Energy,” *Rev. Mod. Phys.*, vol. 75, pp. 559–606, 2003.
- [5] A. G. Riess, L.-G. Sirolder, J. Tonry, S. Casertano, H. C. Ferguson, B. Mobasher, P. Challis, A. V. Filippenko, S. Jha, W. Li, R. Chornock, R. P. Kirshner, B. Leibundgut, M. Dickinson, M. Livio, M. Giavalisco, C. C. Steidel, T. Benítez, and Z. Tsvetanov, “Type ia supernova discoveries at $z > 1$ from the hubble space telescope: Evidence for past deceleration and constraints on dark energy evolution,” *Astrophysical Journal Letters*, vol. 607, no. 2 I, p. 665 – 687, 2004. Cited by: 3258; All Open Access, Bronze Open Access, Green Open Access.
- [6] P. Astier, J. Guy, N. Regnault, R. Pain, E. Aubourg, D. Balam, S. Basa, R. Carlberg, S. Fabbro, F. Dominique, I. Hook, D. Howell, H. Lafoux, J. Neill, N. Palanque-Delabrouille, K. Perrett, C. Pritchett,

- J. Rich, M. Sullivan, and N. Walton, “The supernova legacy survey: measurement of ω_m , ω_Λ and w from the first year data set,” <http://dx.doi.org/10.1051/0004-6361:20054185>, vol. 447, 10 2005.
- [7] D. J. Eisenstein, I. Zehavi, D. W. Hogg, R. Scoccimarro, M. R. Blanton, R. C. Nichol, R. Scranton, H.-J. Seo, M. Tegmark, Z. Zheng, *et al.*, “Detection of the baryon acoustic peak in the large-scale correlation function of sdss luminous red galaxies,” *The Astrophysical Journal*, vol. 633, no. 2, p. 560, 2005.
- [8] C. J. MacTavish, P. A. R. Ade, J. J. Bock, J. R. Bond, J. Borrill, A. Boscaleri, P. Cabella, C. R. Contaldi, B. P. Crill, P. de Bernardis, G. D. Gasperis, A. de Oliveira-Costa, G. D. Troia, G. di Stefano, E. Hivon, A. H. Jaffe, W. C. Jones, T. S. Kisner, A. E. Lange, A. M. Lewis, S. Masi, P. D. Mauskopf, A. Melchiorri, T. E. Montroy, P. Natoli, C. B. Netterfield, E. Pascale, F. Piacentini, D. Pogosyan, G. Polenta, S. Prunet, S. Ricciardi, G. Romeo, J. E. Ruhl, P. Santini, M. Tegmark, M. Veneziani, and N. Vittorio, “Cosmological parameters from the 2003 flight of boomerang,” *The Astrophysical Journal*, vol. 647, p. 799, aug 2006.
- [9] E. Komatsu, J. Dunkley, M. R. Nolta, C. L. Bennett, B. Gold, G. Hinshaw, N. Jarosik, D. Larson, M. Limon, L. Page, D. N. Spergel, M. Halpern, R. S. Hill, A. Kogut, S. S. Meyer, G. S. Tucker, J. L. Weiland, E. Wollack, and E. L. Wright, “Five-year wilkinson microwave anisotropy probe* observations: Cosmological interpretation,” *The Astrophysical Journal Supplement Series*, vol. 180, p. 330, feb 2009.
- [10] M. Tegmark, M. A. Strauss, M. R. Blanton, K. Abazajian, S. Dodelson, H. Sandvik, X. Wang, D. H. Weinberg, I. Zehavi, N. A. Bahcall, *et al.*, “Cosmological parameters from sdss and wmap,” *Physical review D*, vol. 69, no. 10, p. 103501, 2004.
- [11] G. Hinshaw, J. L. Weiland, R. S. Hill, N. Odegard, D. Larson, C. L. Bennett, J. Dunkley, B. Gold, M. R. Greason, N. Jarosik, E. Komatsu, M. R. Nolta, L. Page, D. N. Spergel, E. Wollack, M. Halpern, A. Kogut, M. Limon, S. S. Meyer, G. S. Tucker, and E. L. Wright, “Five-year wilkinson microwave anisotropy probe* observations: Data processing, sky maps, and basic results,” *The Astrophysical Journal Supplement Series*, vol. 180, p. 225, feb 2009.
- [12] G. Risaliti and E. Lusso, “Cosmological constraints from the Hubble diagram of quasars at high redshifts,” *Nature Astron.*, vol. 3, no. 3, pp. 272–277, 2019.
- [13] A. G. Riess, W. Yuan, L. M. Macri, D. Scolnic, D. Brout, S. Casertano, D. O. Jones, Y. Murakami, G. S. Anand, L. Breuval, T. G. Brink, A. V. Filippenko, S. Hoffmann, S. W. Jha, W. D. Kenworthy, J. Mackenty, B. E. Stahl, and W. Zheng, “A comprehensive measurement of the local value of the hubble constant with 1 km/s/mpc uncertainty from the hubble space telescope and the sh0es team,” *The Astrophysical Journal Letters*, vol. 934, p. L7, jul 2022.
- [14] S. Capozziello, Ruchika, and A. A. Sen, “Model independent constraints on dark energy evolution from low-redshift observations,” *Mon. Not. Roy. Astron. Soc.*, vol. 484, p. 4484, 2019.
- [15] E. J. Copeland, M. Sami, and S. Tsujikawa, “Dynamics of dark energy,” *Int. J. Mod. Phys. D*, vol. 15, pp. 1753–1936, 2006.
- [16] P. Bull *et al.*, “Beyond Λ CDM: Problems, solutions, and the road ahead,” *Phys. Dark Univ.*, vol. 12, pp. 56–99, 2016.
- [17] L. Perivolaropoulos and F. Skara, “Challenges for Λ CDM: An update,” *New Astron. Rev.*, vol. 95, p. 101659, 2022.
- [18] N. Schöneberg, G. Franco Abellán, A. Pérez Sánchez, S. J. Witte, V. Poulin, and J. Lesgourgues, “The H0 Olympics: A fair ranking of proposed models,” *Phys. Rept.*, vol. 984, pp. 1–55, 2022.
- [19] I. Zlatev, L.-M. Wang, and P. J. Steinhardt, “Quintessence, cosmic coincidence, and the cosmological constant,” *Phys. Rev. Lett.*, vol. 82, pp. 896–899, 1999.
- [20] T. Chiba, T. Okabe, and M. Yamaguchi, “Kinetically driven quintessence,” *Phys. Rev. D*, vol. 62, p. 023511, 2000.
- [21] R. de Putter and E. V. Linder, “Kinetic k-essence and Quintessence,” *Astropart. Phys.*, vol. 28, pp. 263–272, 2007.
- [22] P. F. Gonzalez-Diaz, “Cosmological models from quintessence,” *Phys. Rev. D*, vol. 62, p. 023513, 2000.
- [23] T. Duany, A. D. N. Banerjee, and N. Banerjee, “Thawing and Freezing Quintessence Models: A thermodynamic Consideration,” *Eur. Phys. J. C*, vol. 79, no. 11, p. 888, 2019.
- [24] R. R. Caldwell and E. V. Linder, “The Limits of quintessence,” *Phys. Rev. Lett.*, vol. 95, p. 141301, 2005.
- [25] S. M. Carroll, “Quintessence and the rest of the world: Suppressing long-range interactions,” *Phys. Rev. Lett.*, vol. 81, pp. 3067–3070, Oct 1998.
- [26] T. Barreiro, O. Bertolami, and P. Torres, “Gamma-Ray Bursts and Dark Energy - Dark Matter interaction,” *Mon. Not. Roy. Astron. Soc.*, vol. 409, pp. 750–754, 2010.
- [27] W. Yang, S. Pan, and A. Paliathanasis, “Cosmological constraints on an exponential interaction in the dark sector,” *Monthly Notices of the Royal Astronomical Society*, vol. 482, pp. 1007–1016, 10 2018.
- [28] R. An, C. Feng, and B. Wang, “Relieving the tension between weak lensing and cosmic microwave background with interacting dark matter and dark energy models,” *Journal of Cosmology and Astroparticle Physics*, vol. 2018, p. 038, feb 2018.

- [29] W. Yang, N. Banerjee, and S. Pan, “Constraining a dark matter and dark energy interaction scenario with a dynamical equation of state,” *Phys. Rev. D*, vol. 95, no. 12, p. 123527, 2017. [Addendum: *Phys.Rev.D* 96, 089903 (2017)].
- [30] S. Fay, “Constraints from growth-rate data on some coupled dark energy models mimicking a Λ CDM expansion,” *Mon. Not. Roy. Astron. Soc.*, vol. 460, no. 2, pp. 1863–1868, 2016.
- [31] W. Yang and L. Xu, “Testing coupled dark energy with large scale structure observation,” *JCAP*, vol. 08, p. 034, 2014.
- [32] A. Piloyan, V. Marra, M. Baldi, and L. Amendola, “Linear perturbation constraints on multi-coupled dark energy,” *Journal of Cosmology and Astroparticle Physics*, vol. 2014, p. 045, feb 2014.
- [33] Y.-H. Li and X. Zhang, “Large-scale stable interacting dark energy model: Cosmological perturbations and observational constraints,” *Phys. Rev. D*, vol. 89, no. 8, p. 083009, 2014.
- [34] W. Yang, S. Pan, E. Di Valentino, R. C. Nunes, S. Vagnozzi, and D. F. Mota, “Tale of stable interacting dark energy, observational signatures, and the H_0 tension,” *JCAP*, vol. 09, p. 019, 2018.
- [35] E. Di Valentino, A. Melchiorri, O. Mena, and S. Vagnozzi, “Interacting dark energy in the early 2020s: A promising solution to the H_0 and cosmic shear tensions,” *Phys. Dark Univ.*, vol. 30, p. 100666, 2020.
- [36] E. Di Valentino, A. Melchiorri, O. Mena, S. Pan, and W. Yang, “Interacting Dark Energy in a closed universe,” *Mon. Not. Roy. Astron. Soc.*, vol. 502, no. 1, pp. L23–L28, 2021.
- [37] A. Gómez-Valent, Z. Zheng, L. Amendola, C. Wetterich, and V. Pettorino, “Coupled and uncoupled early dark energy, massive neutrinos, and the cosmological tensions,” *Phys. Rev. D*, vol. 106, no. 10, p. 103522, 2022.
- [38] B. M. Jackson, A. Taylor, and A. Berera, “On the large-scale instability in interacting dark energy and dark matter fluids,” *Phys. Rev. D*, vol. 79, p. 043526, Feb 2009.
- [39] W. Zimdahl and D. Pavon, “Interacting quintessence,” *Phys. Lett. B*, vol. 521, pp. 133–138, 2001.
- [40] M. S. Linton, A. Pourtsidou, R. Crittenden, and R. Maartens, “Variable sound speed in interacting dark energy models,” *JCAP*, vol. 04, p. 043, 2018.
- [41] G. Olivares, F. Atrio-Barandela, and D. Pavon, “Matter density perturbations in interacting quintessence models,” *Phys. Rev. D*, vol. 74, p. 043521, 2006.
- [42] B. Wang, E. Abdalla, F. Atrio-Barandela, and D. Pavón, “Dark matter and dark energy interactions: theoretical challenges, cosmological implications and observational signatures,” *Reports on Progress in Physics*, vol. 79, p. 096901, aug 2016.
- [43] J. Valiviita, E. Majerotto, and R. Maartens, “Instability in interacting dark energy and dark matter fluids,” *JCAP*, vol. 07, p. 020, 2008.
- [44] D. G. A. Duniya, D. Bertacca, and R. Maartens, “Probing the imprint of interacting dark energy on very large scales,” *Phys. Rev. D*, vol. 91, p. 063530, Mar 2015.
- [45] C. Carbone, M. Baldi, V. Pettorino, and C. Baccigalupi, “Maps of CMB lensing deflection from N-body simulations in Coupled Dark Energy Cosmologies,” *JCAP*, vol. 09, p. 004, 2013.
- [46] L. Amendola and D. Tocchini-Valentini, “Perturbations growth and bias during acceleration,” in *37th Rencontres de Moriond on the Cosmological Model*, pp. 407–410, 5 2002.
- [47] E. R. M. Tarrant, C. van de Bruck, E. J. Copeland, and A. M. Green, “Coupled quintessence and the halo mass function,” *Phys. Rev. D*, vol. 85, p. 023503, Jan 2012.
- [48] J.-H. He and B. Wang, “Effects of the interaction between dark energy and dark matter on cosmological parameters,” *Journal of Cosmology and Astroparticle Physics*, vol. 2008, p. 010, jun 2008.
- [49] J. B. Binder and G. M. Kremer, “Model for a universe described by a non-minimally coupled scalar field and interacting dark matter,” *Gen. Rel. Grav.*, vol. 38, pp. 857–870, 2006.
- [50] T. Patil, S. Panda, M. Sharma, and Ruchika, “Dynamics of interacting scalar field model in the realm of chiral cosmology,” *Eur. Phys. J. C*, vol. 83, no. 2, p. 131, 2023.
- [51] T. Patil and S. Panda, “Coupled scalar field cosmology with effects of curvature,” *Eur. Phys. J. Plus*, vol. 138, no. 7, p. 583, 2023.
- [52] C. van de Bruck, J. Mifsud, J. P. Mimoso, and N. J. Nunes, “Generalized dark energy interactions with multiple fluids,” *JCAP*, vol. 11, p. 031, 2016.
- [53] T. S. Koivisto and N. J. Nunes, “Inflation and dark energy from three-forms,” *Phys. Rev. D*, vol. 80, p. 103509, 2009.
- [54] A. R. Gomes and L. Amendola, “The general form of the coupled Horndeski Lagrangian that allows cosmological scaling solutions,” *JCAP*, vol. 02, p. 035, 2016.
- [55] T. S. Koivisto and N. J. Nunes, “Coupled three-form dark energy,” *Phys. Rev. D*, vol. 88, p. 123512, Dec 2013.
- [56] T. S. Koivisto and N. J. Nunes, “Three-form cosmology,” *Phys. Lett. B*, vol. 685, pp. 105–109, 2010.

- [57] B. J. Barros and N. J. Nunes, “Three-form inflation in type II Randall-Sundrum,” *Phys. Rev. D*, vol. 93, no. 4, p. 043512, 2016.
- [58] N. Aghanim *et al.*, “Planck 2018 results. VI. Cosmological parameters,” *Astron. Astrophys.*, vol. 641, p. A6, 2020. [Erratum: *Astron. Astrophys.* 652, C4 (2021)].
- [59] D. Dutcher *et al.*, “Measurements of the E-mode polarization and temperature-E-mode correlation of the CMB from SPT-3G 2018 data,” *Phys. Rev. D*, vol. 104, no. 2, p. 022003, 2021.
- [60] S. Aiola *et al.*, “The Atacama Cosmology Telescope: DR4 Maps and Cosmological Parameters,” *JCAP*, vol. 12, p. 047, 2020.
- [61] L. Verde, T. Treu, and A. G. Riess, “Tensions between the Early and the Late Universe,” *Nature Astron.*, vol. 3, p. 891, 7 2019.
- [62] J. Evslin, A. A. Sen, and Ruchika, “Price of shifting the Hubble constant,” *Phys. Rev. D*, vol. 97, no. 10, p. 103511, 2018.
- [63] S. Kumar and R. C. Nunes, “Echo of interactions in the dark sector,” *Phys. Rev. D*, vol. 96, no. 10, p. 103511, 2017.
- [64] W. Yang, A. Mukherjee, E. Di Valentino, and S. Pan, “Interacting dark energy with time varying equation of state and the H_0 tension,” *Phys. Rev. D*, vol. 98, no. 12, p. 123527, 2018.
- [65] E. Di Valentino, O. Mena, S. Pan, L. Visinelli, W. Yang, A. Melchiorri, D. F. Mota, A. G. Riess, and J. Silk, “In the realm of the Hubble tension—a review of solutions,” *Class. Quant. Grav.*, vol. 38, no. 15, p. 153001, 2021.
- [66] F. Okamoto, T. Sekiguchi, and T. Takahashi, “ H_0 tension without CMB data: Beyond the Λ CDM,” *Phys. Rev. D*, vol. 104, no. 2, p. 023523, 2021.
- [67] E. Di Valentino *et al.*, “Cosmology Intertwined III: $f\sigma_8$ and S_8 ,” *Astropart. Phys.*, vol. 131, p. 102604, 2021.
- [68] V. Salvatelli, N. Said, M. Bruni, A. Melchiorri, and D. Wands, “Indications of a late-time interaction in the dark sector,” *Phys. Rev. Lett.*, vol. 113, no. 18, p. 181301, 2014.
- [69] J. Väliiviita and E. Palmgren, “Distinguishing interacting dark energy from Λ CDM with CMB, lensing, and baryon acoustic oscillation data,” *JCAP*, vol. 07, p. 015, 2015.
- [70] R. C. Nunes, S. Pan, and E. N. Saridakis, “New constraints on interacting dark energy from cosmic chronometers,” *Phys. Rev. D*, vol. 94, no. 2, p. 023508, 2016.
- [71] E. Marachlian, I. E. Sánchez G., and O. P. Santillán, “Emergent Universe as an interaction in the dark sector,” *Mod. Phys. Lett. A*, vol. 32, no. 28, p. 1750152, 2017.
- [72] A. Banerjee, H. Cai, L. Heisenberg, E. O. Colgáin, M. M. Sheikh-Jabbari, and T. Yang, “Hubble sinks in the low-redshift swampland,” *Phys. Rev. D*, vol. 103, no. 8, p. L081305, 2021.
- [73] B.-H. Lee, W. Lee, E. O. Colgáin, M. M. Sheikh-Jabbari, and S. Thakur, “Is local H_0 at odds with dark energy EFT?,” *JCAP*, vol. 04, no. 04, p. 004, 2022.
- [74] G. Montani, M. De Angelis, F. Bombacigno, and N. Carlevaro, “Metric $f(R)$ gravity with dynamical dark energy as a paradigm for the Hubble Tension,” 6 2023.
- [75] M. Archidiacono, E. Castorina, D. Redigolo, and E. Salvioni, “Unveiling dark fifth forces with linear cosmology,” *JCAP*, vol. 10, p. 074, 2022.
- [76] T. Koivisto, D. Wills, and I. Zavala, “Dark D-brane Cosmology,” *JCAP*, vol. 06, p. 036, 2014.
- [77] D. Chowdhury, G. Tasinato, and I. Zavala, “Dark energy, D-branes, and Pulsar Timing Arrays,” 7 2023.
- [78] L. Knox and M. Millea, “Hubble constant hunter’s guide,” *Phys. Rev. D*, vol. 101, no. 4, p. 043533, 2020.
- [79] E. Di Valentino *et al.*, “Snowmass2021 - Letter of interest cosmology intertwined II: The hubble constant tension,” *Astropart. Phys.*, vol. 131, p. 102605, 2021.
- [80] A. A. Sen, S. A. Adil, and S. Sen, “Do cosmological observations allow a negative Λ ?,” *Mon. Not. Roy. Astron. Soc.*, vol. 518, no. 1, pp. 1098–1105, 2022.
- [81] L. A. Escamilla, O. Akarsu, E. Di Valentino, and J. A. Vazquez, “Model-independent reconstruction of the Interacting Dark Energy Kernel: Binned and Gaussian process,” 2023.
- [82] S. A. Adil, O. Akarsu, E. Di Valentino, R. C. Nunes, E. Ozulker, A. A. Sen, and E. Specogna, “Omnipotent dark energy: A phenomenological answer to the Hubble tension,” 2023.
- [83] M. Rezaei and J. Sola Peracaula, “Running vacuum versus holographic dark energy: a cosmographic comparison,” *Eur. Phys. J. C*, vol. 82, no. 8, p. 765, 2022.
- [84] M. Rezaei, J. Solà Peracaula, and M. Malekjani, “Cosmographic approach to Running Vacuum dark energy models: new constraints using BAOs and Hubble diagrams at higher redshifts,” *Mon. Not. Roy. Astron. Soc.*, vol. 509, no. 2, pp. 2593–2608, 2021.

- [85] M. Rezaei, M. Malekjani, and J. Sola, “Can dark energy be expressed as a power series of the Hubble parameter?,” *Phys. Rev. D*, vol. 100, no. 2, p. 023539, 2019.
- [86] L. Amendola, “Coupled quintessence,” *Phys. Rev. D*, vol. 62, p. 043511, Jul 2000.
- [87] L. Amendola and D. Tocchini-Valentini, “Baryon bias and structure formation in an accelerating universe,” *Phys. Rev. D*, vol. 66, p. 043528, 2002.
- [88] T. Damour and C. Gundlach, “Nucleosynthesis constraints on an extended jordan-brans-dicke theory,” *Phys. Rev. D*, vol. 43, pp. 3873–3877, Jun 1991.
- [89] L. Chen, Q.-G. Huang, and K. Wang, “Distance Priors from Planck Final Release,” *JCAP*, vol. 02, p. 028, 2019.
- [90] P. A. R. Ade *et al.*, “Planck 2015 results. XIV. Dark energy and modified gravity,” *Astron. Astrophys.*, vol. 594, p. A14, 2016.
- [91] D. Scolnic *et al.*, “The Pantheon+ Analysis: The Full Data Set and Light-curve Release,” *Astrophys. J.*, vol. 938, no. 2, p. 113, 2022.
- [92] D. Brout *et al.*, “The Pantheon+ Analysis: Cosmological Constraints,” *Astrophys. J.*, vol. 938, no. 2, p. 110, 2022.
- [93] A. G. Riess *et al.*, “A Comprehensive Measurement of the Local Value of the Hubble Constant with 1 km/s/Mpc Uncertainty from the Hubble Space Telescope and the SH0ES Team,” *Astrophys. J. Lett.*, vol. 934, no. 1, p. L7, 2022.
- [94] M. Moresco, A. Cimatti, R. Jimenez, and et. al, “Improved constraints on the expansion rate of the universe up to $z = 1.1$ from the spectroscopic evolution of cosmic chronometers,” *Journal of Cosmology and Astroparticle Physics*, vol. 2012, no. 08, p. 006–006, 2012.
- [95] M. Moresco, “Raising the bar: new constraints on the Hubble parameter with cosmic chronometers at $z \sim 2$,” *Mon. Not. Roy. Astron. Soc.*, vol. 450, no. 1, pp. L16–L20, 2015.
- [96] M. Moresco, L. Pozzetti, A. Cimatti, R. Jimenez, C. Maraston, L. Verde, D. Thomas, A. Citro, R. Tojeiro, and D. Wilkinson, “A 6% measurement of the Hubble parameter at $z \sim 0.45$: direct evidence of the epoch of cosmic re-acceleration,” *JCAP*, vol. 05, p. 014, 2016.
- [97] F. Beutler *et al.*, “The 6df galaxy survey: baryon acoustic oscillations and the local hubble constant,” *Monthly Notices of the Royal Astronomical Society*, vol. 416, pp. 3017–3032, jul 2011.
- [98] A. J. Ross, L. Samushia, C. Howlett, W. J. Percival, A. Burden, and M. Manera, “The clustering of the SDSS DR7 main Galaxy sample – I. A 4 per cent distance measure at $z = 0.15$,” *Mon. Not. Roy. Astron. Soc.*, vol. 449, no. 1, pp. 835–847, 2015.
- [99] M. Ata *et al.*, “The clustering of the SDSS-IV extended Baryon Oscillation Spectroscopic Survey DR14 quasar sample: first measurement of baryon acoustic oscillations between redshift 0.8 and 2.2,” *Mon. Not. Roy. Astron. Soc.*, vol. 473, no. 4, pp. 4773–4794, 2018.
- [100] H. du Mas des Bourboux *et al.*, “Baryon acoustic oscillations from the complete SDSS-III Ly α -quasar cross-correlation function at $z = 2.4$,” *Astron. Astrophys.*, vol. 608, p. A130, 2017.
- [101] S. Alam *et al.*, “The clustering of galaxies in the completed SDSS-III Baryon Oscillation Spectroscopic Survey: cosmological analysis of the DR12 galaxy sample,” *Mon. Not. Roy. Astron. Soc.*, vol. 470, no. 3, pp. 2617–2652, 2017.
- [102] M. J. Reid, J. A. Braatz, J. J. Condon, L. J. Greenhill, C. Henkel, and K. Y. Lo, “The megamaser cosmology project. i. very long baseline interferometric observations of ugc 3789,” *The Astrophysical Journal*, vol. 695, p. 287, mar 2009.
- [103] J. A. Braatz, M. J. Reid, E. M. L. Humphreys, C. Henkel, J. J. Condon, and K. Lo, “The megamaser cosmology project. ii. the angular-diameter distance to ugc 3789,” *The Astrophysical Journal*, vol. 718, p. 657, jul 2010.
- [104] M. J. Reid, J. A. Braatz, J. J. Condon, K. Y. Lo, C. Y. Kuo, C. M. V. Impellizzeri, and C. Henkel, “The megamaser cosmology project. iv. a direct measurement of the hubble constant from ugc 3789,” *The Astrophysical Journal*, vol. 767, p. 154, apr 2013.
- [105] C. Y. Kuo, J. A. Braatz, M. J. Reid, K. Y. Lo, J. J. Condon, C. M. V. Impellizzeri, and C. Henkel, “The megamaser cosmology project. v. an angular-diameter distance to ngc 6264 at 140 mpc,” *The Astrophysical Journal*, vol. 767, p. 155, apr 2013.
- [106] F. Gao, J. A. Braatz, M. J. Reid, K. Y. Lo, J. J. Condon, C. Henkel, C. Y. Kuo, C. M. V. Impellizzeri, D. W. Pesce, and W. Zhao, “The megamaser cosmology project. viii. a geometric distance to ngc 5765b,” *The Astrophysical Journal*, vol. 817, p. 128, jan 2016.
- [107] S. Basilakos, S. Nesseris, and L. Perivolaropoulos, “Observational constraints on viable $f(R)$ parametrizations with geometrical and dynamical probes,” *Phys. Rev. D*, vol. 87, no. 12, p. 123529, 2013.
- [108] D. Foreman-Mackey, D. W. Hogg, D. Lang, and J. Goodman, “emcee: The mcmc hammer,” *Publications of the Astronomical Society of the Pacific*, vol. 125, p. 306, feb 2013.

- [109] C. Heymans *et al.*, “KiDS-1000 Cosmology: Multi-probe weak gravitational lensing and spectroscopic galaxy clustering constraints,” *Astron. Astrophys.*, vol. 646, p. A140, 2021.
- [110] T. M. C. Abbott and et al., “Joint analysis of dark energy survey year 3 data and cmb lensing from spt and planck. iii. combined cosmological constraints,” *Phys. Rev. D*, vol. 107, p. 023531, Jan 2023.
- [111] J. L. Bernal, L. Verde, and A. G. Riess, “The trouble with H_0 ,” *JCAP*, vol. 10, p. 019, 2016.
- [112] V. de Sainte Agathe *et al.*, “Baryon acoustic oscillations at $z = 2.34$ from the correlations of Ly α absorption in eBOSS DR14,” *Astron. Astrophys.*, vol. 629, p. A85, 2019.